

Copper isotope fractionation during asteroid core solidification

P. Ni, Y. Zhan, N.L. Chabot, C.J. Ryan, K. Zhu, N.X. Nie, S.B. Shirey, A. Shahar

Supplementary Information

The Supplementary Information includes:

- 1. Solid-liquid metal equilibrium experiments for Cu
- 2. Electron microprobe analyses
- 3. Copper isotope analyses
- 4. Calculating apparent equilibrium temperature for Fe isotope fractionation between metal and troilite
- 5. Lessons learned for equilibrium Cu isotope fractionation experiments
- 6. Modelling of Cu redistribution between metal and troilite during cooling of the iron meteorite parent body
- Tables S-1 to S-3
- Figures S-1 to S-5
- Supplementary Information References

1. Solid-liquid metal equilibrium experiments for Cu

The solid-liquid metal equilibrium experiments were conducted at the Johns Hopkins University Applied Physics Laboratory following a similar approach as in Chabot *et al.* (2017). High-purity Fe, Ni, and FeS powders were mixed and doped with approximately 1 wt. % Cu powder. For experiments S25-Cu1, S25-Cu2, S25-Cu3, S15-Cu1, S10-Cu1, and S5-Cu1, a small amount of Ru, Os, and W were doped in the starting mixture for separate purposes (Table S-1). For each of the 10 experiments, appropriate amounts of the starting mixtures were weighed and sealed in a high-purity silica tube that was connected to vacuum. Experiments were conducted using a one-atmosphere vertical furnace at temperatures of 1260 to 1425 °C. The duration of the experiments was between 1 and 6 days. At the end of the experiments, the silica tube was removed from the furnace and quenched in water. The experimental samples were subsequently recovered from the tube and mounted in epoxy for preservation. After being sliced into multiple sections using a diamond saw, cross sections of the sample were mounted in epoxy again and polished to achieve a smooth surface for analyses.

2. Electron microprobe analyses

Electron microprobe analyses were conducted to measure major element compositions of the experimental samples for Fe, Ni, S, and Cu at the Carnegie Institution for Science using a JEOL 8530 F electron microprobe. A 15 kV, 20 nA beam was defocused to 100 µm for the quenched solid and metal phases in the experiments. The large beam diameter was important to compensate for the chemical heterogeneities caused by the quench textures in the liquid metal phase, as shown in Figure S-1. The counting time was 30 s for Ni, Fe and Cu and

60 s for S. For each phase of the experiments, approximately 10 to 20 analyses were conducted and the errors were reported as two standard deviations of the mean. For the liquid metal phase, however, errors were reported as two standard errors of the mean to average out uncertainties caused by the dendritic quench textures.

3. Copper isotope analyses

The solid and liquid metal phases of the experiments were sampled using a Newwave micromill for Cu isotope analyses. The samples were cleaned in an ultrasonic bath of deionized water prior to drilling. A new tungsten carbide drill bit 300 to 700 μm in diameter was used for each phase to avoid cross-contamination. Each drill hole was 400 to 500 μm in depth. For phases with low concentrations of Cu, materials from multiple drill holes were combined to ensure the recovery of sufficient amount of Cu for analyses. A drop of Milli-Q water was placed at the target position before drilling to help collect the drilled particles with the surface tension of water. The drilled particles were suspended in the Milli-Q and transferred to a Teflon vial using a pipette. A few drops of Milli-Q water were placed near the drill site to help transfer the residual particles afterwards and the process was repeated multiple times. The sample surface was always cleaned with Milli-Q water and compressed air before being used for drilling the next phase. Since the liquid metal phases have higher concentrations of Cu, sampling of each experimental charge was always started with the solid metal and then the liquid metal. After micromill sampling, the drilled holes were examined with an optical microscope to ensure they only penetrated one phase as originally planned.

The drilled particles were dried down on a hot plate, and dissolved in 1 ml concentrated HCl + 0.5 ml concentrated HNO₃ on a hot plate for at least 24 hours. After complete dissolution was achieved, the sample was dried down and small amounts of concentrated HCl was added to the Teflon vials to drive away NO₃⁻ introduced during the dissolution. Chemical purification of Cu was performed using established lab procedures previously published in Ni *et al.* (2021). In-house custom-made quartz glass columns 0.4 cm in diameter were loaded with approximately 7.5 cm of BioRad AG1-X8 (200-400 mesh) resin for Cu purification. After being converted to the chloride form, dissolved samples were loaded on the column in 8 M HCl + 0.001% H₂O₂. Then 7 ml of 8 M HCl + 0.001% H₂O₂ was added to remove most of the matrix elements. The Cu fraction of the column was then collected by eluting 9 ml of 8 M HCl + 0.001% H₂O₂. The above procedure was repeated once to achieve cleaner separation of Cu from the matrix elements. Two milliliters of eluents before and after the Cu fraction of the column were collected separately to monitor any potential shift of the Cu peak and to ensure the recovery rate was >99%. The blank of the column procedure was 0.5 ng, significantly lower than the amount of Cu yielded in each sample (250 ng to 50 μg).

Copper isotope analyses were conducted using the Nu Plasma II at the Carnegie Institution for Science. The instrument was operated at low mass resolution in wet plasma mode. Samples and standards were diluted to 50 or 100 ppb in 0.4 M HNO₃ for analyses and the sensitivity was 25-40 V/ppm for ⁶³Cu. Each sample was analysed 4 to 10 times and each measurement consisted of 20 cycles with 4 s integrations. ERM-AE633 was used as the isotope standard for sample-standard bracketing to correct for instrumental mass bias. The measured Cu isotope ratios are reported relative to NIST SRM 976 after correcting a -0.01‰ difference between the two isotope standards (ERM-AE633 and NIST SRM 976, Moeller *et al.*, 2012):

$$\begin{aligned}\delta^{65}\text{Cu} (\text{‰}) &= \left[\left(\frac{^{65}\text{Cu}}{^{63}\text{Cu}} \right)_{\text{Sample}} / \left(\frac{^{65}\text{Cu}}{^{63}\text{Cu}} \right)_{\text{SRM976}} - 1 \right] \times 1000 \\ &= \left[\left(\frac{^{65}\text{Cu}}{^{63}\text{Cu}} \right)_{\text{Sample}} / \left(\frac{^{65}\text{Cu}}{^{63}\text{Cu}} \right)_{\text{AE633}} - 1 \right] \times 1000 + 0.01.\end{aligned}$$

4. Calculating apparent equilibrium temperature for Fe isotope fractionation between metal and troilite

Apparent equilibrium temperatures for Fe isotope fractionation between metal and troilite in iron meteorites were calculated using published reduced partition function ratio for α -Fe (bcc) and troilite (Dauphas *et al.*, 2012, 2017). The equilibrium fractionation factor for α -Fe (bcc) was calculated using:

$$1000\ln\beta_{\alpha\text{-Fe}}(^{56}\text{Fe}/^{54}\text{Fe}) = 0.49970 \times 10^6/T^2 - 1.14240 \times 10^9/T^4,$$

while that for troilite was using:

$$1000\ln\beta_{\text{troilite}}(^{56}\text{Fe}/^{54}\text{Fe}) = 0.29101 \times 10^6/T^2 - 0.63530 \times 10^9/T^4.$$

In the above equations T is the temperature in K.

Equilibrium isotope fractionation between metal and troilite was subsequently calculated via:

$$\Delta_{56/54}(\alpha\text{-Fe/troilite}) = 1000\ln\beta_{\alpha\text{-Fe}}(^{56}\text{Fe}/^{54}\text{Fe}) - 1000\ln\beta_{\text{troilite}}(^{56}\text{Fe}/^{54}\text{Fe}).$$

And $\Delta_{57/54}(\alpha\text{-Fe/troilite})$ was calculated assuming mass-dependent fractionation of the three isotopes of iron following the equilibrium fractionation law (Young *et al.*, 2002):

$$\begin{aligned} \Delta_{57/54}(\alpha\text{-Fe/troilite}) &= (1/M_{54} - 1/M_{57}) / (1/M_{54} - 1/M_{56}) \times \Delta_{56/54}(\alpha\text{-Fe/troilite}) \\ &= 1.475 \times \Delta_{56/54}(\alpha\text{-Fe/troilite}). \end{aligned}$$

The calculated apparent equilibrium temperatures (T_{ae}) are plotted in Figure 3.

5. Lessons learned for equilibrium isotope fractionation experiments

Our experiments have profound implications for equilibrium isotope fractionation experiments. First, our data unambiguously show that elemental equilibrium cannot be used to indicate isotope equilibrium. As shown in Figure S-2, all 10 experiments yielded Cu partition coefficients consistent with literature data. But careful evaluation of isotopic equilibrium demonstrated that the five experiments at higher temperatures have experienced evaporative Cu loss, leading to kinetic isotope fractionation. Copper was lost from the liquid metal during evaporation, causing Cu to diffuse from solid metal into liquid metal to maintain equilibrium. But this was limited by Cu diffusion in solid metal and caused the measured partition coefficients to be on the high end of the data (Figure S-2). This process led to limited departure from equilibrium Cu partitioning that is hard to distinguish from experimental errors, but the effect on Cu isotope fractionation is quite significant. The diffusive reequilibrium caused the liquid metal to become higher in $^{65}\text{Cu}/^{63}\text{Cu}$ ratio over time and the solid metal to show isotopic heterogeneity (Figure S-4, Table S-2). This finding indicates the importance of the closed system test for isotope equilibrium experiments. If a sink or a source of the target element exists in the system, it might reach a steady state instead of true equilibrium. At such steady states, element partition could still reach near-equilibrium, but isotope exchange would be dominated by kinetic fractionation.

Second, for isotope systems like Cu that only contain two stable isotopes, the “three-isotope” technique cannot be applied to test for isotopic equilibrium (Shahar *et al.*, 2017), making it especially important to check for closed system behavior of the element and conduct time-series experiments. Based on a combination of both tests, we were able to distinguish experiments in our study that did not reach isotope equilibrium. Unfortunately, these methods have not been specifically employed in previous experiments for equilibrium Cu isotope fractionation (Savage *et al.*, 2015; Xia *et al.*, 2019), making it less convincing that isotopic equilibrium has been reached in these experiments. The exact cause for the Cu loss trend in our non-equilibrated experiments (Figure S-4) is unclear, but we suspect it was the consequence of multiple factors: 1) effect of temperature and sulphur content on Cu volatility; 2) duration of the experiment; and 3) surface area of the liquid metal exposed for evaporation.

Third, our data demonstrate how deceiving trends could appear for experiments that are dominated by kinetic isotope fractionation. As plotted in Figure S-5, the five experiments affected by evaporative Cu loss appear to have a linear correlation between $\Delta^{65}\text{Cu}$ and S content of the liquid metal, except for one data point that falls slightly off the trend (S15-Cu2). Note that this trend is completely artificial but could misguide ones to believe that these experiments have reached isotopic equilibrium. In fact, it is quite possible for kinetically controlled isotope exchange experiments to show temperature dependence. This is because diffusion and chemical reaction rates are also temperature dependent. For a non-equilibrium system, it is possible that it reaches closer to equilibrium fractionation at higher temperatures but further away from equilibrium at lower temperatures. This temperature effect could lead to a larger apparent isotopic fractionation between two phases at lower temperatures but a smaller fractionation at higher temperatures, which is coincidentally the expectation for equilibrium fractionation. Therefore, judging whether experiments have reached isotopic equilibrium based on the final trend of the data could be misleading.

Overall, our experiments strongly support the necessity of independently verifying isotopic equilibrium for isotope exchange experiments. For isotope systems that contain only two stable isotopes, it is especially important to test for closed system behavior of the target element and conduct time series experiments to check for isotopic equilibrium.

6. Modelling of Cu redistribution between metal and troilite during cooling of the iron meteorite parent body

Assuming a spherical troilite with fixed radius of a exchanging Cu with matrix metal in a finite radius of b , the governing equation describing Cu diffusion in one-dimensional spherical coordinate is:

$$\frac{\partial C}{\partial t} = \frac{D}{r^2} \frac{\partial}{\partial r} \left(r^2 \frac{\partial C}{\partial r} \right) |_{a \leq r \leq b},$$

with boundary conditions of:

$$\begin{aligned} \frac{\partial C}{\partial r} |_{r=b} &= 0, \\ C(t) |_{r=a} &= \kappa C_{FeS}(t), \\ \text{and } dC_{FeS} &= \frac{\int_a^b 4\pi r^2 \rho_{Metal}(C - C_0) dr}{4/3\pi a^3 \rho_{FeS}}. \end{aligned}$$

In the above equation, D is the diffusivity, r is the radial distance, C is the concentration in the metal matrix, κ is Cu partition coefficient between metal and troilite, ρ_{Metal} and ρ_{FeS} are densities of metal and troilite, C_0 is the initial concentration in metal, and C_T is the concentration in the troilite and assumed to be homogeneous. Copper diffusion in sulphide (Cherniak, 2010) is orders of magnitude faster than in metal (Salje and Feller-Kniepmeier, 1977), making it possible to reach a homogeneous composition in the troilite when exchanging Cu with the metal matrix.

The key parameters needed to solve the above equations are the diffusivity of Cu (D) and the Cu partition coefficient (κ), which are both functions of temperature. Copper diffusivity in iron metal has been experimentally determined (Salje and Feller-Kniepmeier, 1977) and re-fitted to be:

$$D = D_0 \exp\left(-\frac{E_0}{RT}\right) = 0.03 \exp\left(\frac{283675 \text{ J/mol}}{RT}\right) \text{ m}^2/\text{s}.$$

In the above equation, D_0 is the pre-exponential term in m^2/s , E_0 is the activation energy for diffusion, and R is the gas constant which equals 8.314 J/mol/K.

Experimental data on Cu partitioning between metal and troilite (κ) are limited. A recent study found κ to be 1 for Cu at the solid metal-liquid metal-troilite cotectic (Shread *et al.*, 2024), which also agrees with the observed apparent κ in iron meteorites with high cooling rates (Figure 3). Therefore, we fix $\kappa = 1$ at 1200 K and convert Eq. (3) into the form of:

$$\ln \kappa = -\frac{B}{T_0} + \frac{B}{T},$$

in which $T_0 = 1200$ K and B is an adjustable parameter that determines how strongly κ depends on temperature. At $T = T_0$, κ always have a value of 1 regardless the value of B .

The thermal history of the iron meteorite parent bodies is simulated using the asymptotic cooling model:

$$T = \frac{T_0 - T_c}{1 + \frac{t}{\tau_c}} + T_c,$$

where T_0 is the initial temperature, T_c is the terminal temperature, t is time, and τ_c is the cooling time scale. In order to calculate isotopic fractionation of ^{63}Cu and ^{65}Cu , they were assumed to have the same partition coefficient between metal and troilite (i.e., $\kappa_{63\text{Cu}} = \kappa_{65\text{Cu}} = \kappa_{\text{Cu}}$, no equilibrium isotope fractionation), but different diffusivities as a function of their mass:

$$\frac{D_{63\text{Cu}}}{D_{65\text{Cu}}} = \left(\frac{M_{65}}{M_{63}}\right)^\beta = \left(\frac{64.927789}{62.929597}\right)^\beta.$$

In the above equation, β ($0 \leq \beta \leq 0.5$) is an empirical parameter that describes how the two isotopes of Cu fractionate by diffusion. Existing data for Cu diffusion in Al, Cu, CuZn, Li, and Pb yielded a large range of β values from 0.1 to 0.45, making it difficult to predict how Cu would behave in Fe metal. Therefore, a β value of 0.5 is used to explore the maximum effect of kinetic fractionation for Cu isotopes.

In each simulation, the concentration profiles of ^{63}Cu and ^{65}Cu were solved independently and their ratios along the profile were compared with the initial ratio to obtain isotopic fractionation expressed in delta notations:

$$\delta^{65}\text{Cu}(r, t) = \left(\frac{^{65}\text{Cu}(r, t)/^{63}\text{Cu}(r, t)}{(^{65}\text{Cu}/^{63}\text{Cu})_0} - 1\right) \times 1000\text{‰},$$

where $(^{65}\text{Cu}/^{63}\text{Cu})_0$ is the initial Cu isotopic ratio, which is assumed to be homogenous throughout the system at $t = 0$.

A list of all parameters required to reproduce our model is provided in Table S-3. A troilite radius of 2 mm was chosen for the model based on the average size of troilite grains analysed in Williams and Archer (2011). The effective matrix radius was assumed to be 5, 10, or 20 times that of the troilite. The value of B for the temperature dependence of the partition coefficient is unknown and remains a large uncertainty of the model. A B value of -75,000 was arbitrarily chosen based on test model runs that showed the maximum effect of kinetic fractionation.

With the above boundary conditions and initial conditions, the governing one-dimensional diffusion equation was solved numerically using a COMSOL Multiphysics 6.0. The model was first performed at a fixed temperature for a given duration to benchmark with the analytical solution, before being applied to the temperature-dependent situations.

Supplementary Tables

Table S-1 Run conditions and chemical compositions for all ten solid-liquid metal experiments. Concentrations are in wt. %. Errors are given in 2 standard deviations for the solid metal, but in 2 standard errors for the liquid metal phase to account for the chemical heterogeneity caused by quench textures.

Exp #	Phase	T (°C)	t (days)	Fe	Ni	S	Cu	Total
S25-Cu1*	Solid	1260	5	86.39±0.41	12.14±0.12	0.04±0.01	0.36±0.03	98.58±0.43
	Liquid			62.68±0.90	7.35±0.46	26.08±0.94	1.68±0.14	96.11±1.38
S25-Cu2*	Solid	1260	2.75	85.91±0.55	12.49±0.13	0.03±0.01	0.37±0.02	98.43±0.57
	Liquid			59.93±0.66	7.09±0.36	28.46±0.59	3.31±0.25	95.47±0.99
S25-Cu3*	Solid	1260	1	82.34±0.86	11.95±0.21	0.04±0.01	0.36±0.04	94.33±0.89
	Liquid			59.68±1.38	7.15±0.41	26.16±1.43	2.63±0.25	93.00±2.04
S20-Cu1*	Solid	1300	6	86.12±0.51	12.30±0.09	0.03±0.01	0.37±0.05	98.46±0.52
	Liquid			62.08±0.83	7.63±0.50	27.10±1.01	2.46±0.13	96.81±1.41
S15-Cu1*	Solid	1350	1	86.73±0.43	12.00±0.09	0.04±0.01	0.49±0.05	98.76±0.44
	Liquid			65.49±1.19	9.16±0.28	22.09±0.90	1.68±0.14	96.73±1.52
S15-Cu2	Solid	1370	1	89.15±0.67	9.77±0.14	0.05±0.01	0.44±0.04	99.40±0.34
	Liquid			74.00±0.23	9.32±0.09	14.86±0.33	1.35±0.07	99.53±0.42
S15-Cu6	Solid	1380	2.75	90.62±0.47	9.00±0.07	0.05±0.02	0.46±0.03	100.13±0.26
	Liquid			79.48±0.28	8.93±0.05	10.90±0.25	1.02±0.03	100.33±0.38
S10-Cu1*	Solid	1380	4	87.25±0.65	10.52±0.16	0.04±0.02	0.47±0.04	97.81±0.67
	Liquid			73.46±0.56	10.08±0.04	14.41±0.33	1.39±0.06	97.94±0.66
S5-Cu1*	Solid	1425	1	88.71±0.25	10.10±0.13	0.04±0.01	0.60±0.08	98.84±0.28
	Liquid			83.38±0.44	10.80±0.07	4.39±0.49	0.97±0.06	98.57±0.66
S5-Cu3	Solid	1400	1	88.32±0.76	9.86±0.08	0.04±0.01	0.46±0.04	98.68±0.41
	Liquid			81.54±0.30	10.29±0.06	6.26±0.39	0.80±0.06	98.90±0.50

*These experiments were doped with a few weight percent of Os, W, and Ru for separate purposes. The totals of the solid metal and liquid metal phases in these experiments do not account for these three elements and could hence be significantly lower than 100 wt. %.

Table S-2 Copper isotope compositions for the solid–liquid metal equilibrium experiment products. Errors are reported in two standard errors of 4 to 10 analyses.

Exp #	Phase	T (°C)	t (days)	$\delta^{65}\text{Cu}$ (‰)	n	$\Delta^{65}\text{Cu}_{\text{sol-liq metal}}$ (‰)
S25-Cu1	Solid	1260	5	0.43±0.07	5	-0.02±0.14
	Liquid			0.46±0.10	4	
S25-Cu2	Solid	1260	2.75	0.47±0.04	10	-0.02±0.06
	Liquid			0.49±0.04	9	
S25-Cu3	Solid	1260	1	0.38±0.04	10	0.03±0.06
	Liquid			0.35±0.04	10	
S20-Cu1	Solid	1300	6	0.68±0.03	8	0.00±0.04
	Liquid			0.69±0.02	8	
S15-Cu1	Solid	1350	1	0.65±0.03	8	0.03±0.06
	Liquid			0.62±0.04	8	
S15-Cu2	Solid	1370	1	1.39±0.19	4	<i>Not equilibrated</i>
	Liquid			1.75±0.08	4	
	Tube leachate			-1.51±0.06	8	
S15-Cu6	Solid	1380	2.75	0.92±0.08	4	<i>Not equilibrated</i>
	Liquid			1.29±0.11	4	
S10-Cu1	Solid	1380	4	0.81±0.03	6	<i>Not equilibrated</i>
	<i>duplicate</i>			0.91±0.02	4	
	Liquid			1.60±0.05	6	
	<i>duplicate</i>			1.54±0.03	4	
S5-Cu1	Solid	1425	1	0.54±0.04	6	<i>Not equilibrated</i>
	<i>duplicate</i>			0.72±0.02	4	
	Liquid			0.75±0.02	6	
	<i>duplicate</i>			0.79±0.03	4	
S5-Cu3	Solid	1400	1	0.71±0.06	8	<i>Not equilibrated</i>
	Liquid			0.92±0.05	8	
S15-Cu1 initial powder	N/A	N/A	N/A	0.44±0.02	10	N/A
Cu powder	N/A	N/A	N/A	0.45±0.02	8	N/A

Table S-3 List of parameters and their values used in the model for Cu exchange between metal–troilite and the consequences for Cu isotope fractionation during cooling of iron meteorite parent bodies.

Symbol	Description	Value	Unit
D_0	Pre-exponential factor for Cu diffusivity in iron metal	0.03	m ² /s
E_0	Activation Energy for Cu diffusivity in iron metal	283675	J/mol
T_0	Initial temperature	1200	K
T_c	Terminal temperature	600	K
C_0	Initial concentration of Cu in the metal matrix	1	Dimensionless
ρ_{FeS}	Density of the troilite	4610	kg/m ³
ρ_{Metal}	Density of iron metal	7870	kg/m ³
a	Radius of the troilite grain	2	mm
b	Radius of the iron meteorite matrix exchanging with troilite	10, 20, 40	mm
B	Coefficient for temperature dependence of κ	-7.5×10^4	K
β	Factor for Cu isotope fractionation by	0.5	Dimensionless
τ_c	Cooling time scale	0.001 to 100	Myr

Supplementary Figures

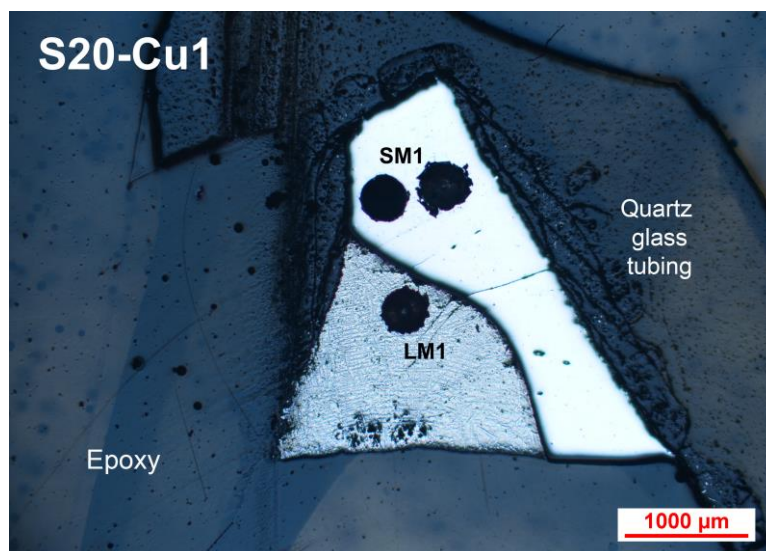


Figure S-1 Microscopic image of an experimental charge (S20-Cu1) after being sliced, preserved in epoxy, and sampled by a micromill for Cu isotope analyses. The drill holes on the solid metal and quenched liquid metal are marked as “SM1” and “LM1”, respectively. The quenched liquid metal shows dendritic quench textures typical of this type of experiments.

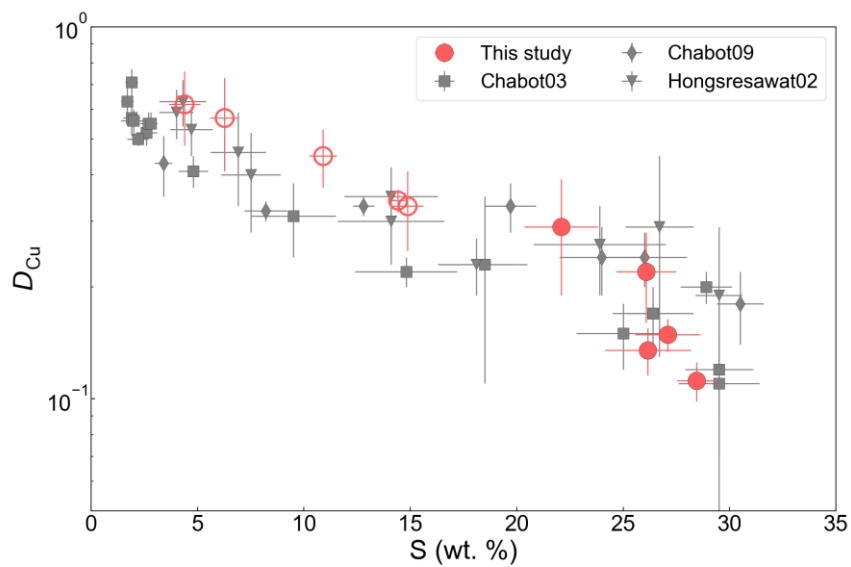


Figure S-2 Measured Cu partition coefficients between solid metal and liquid metal in this study compared with literature data. All 10 experiments appear to have reached equilibrium in Cu partitioning between the two phases. Experiments that show isotopic disequilibrium are plotted in open symbols. Sulphur content on the x-axis refers to that of the liquid metal. Error bars represent one standard deviation. Literature data are from (Chabot and Jones, 2003; Chabot *et al.*, 2009).

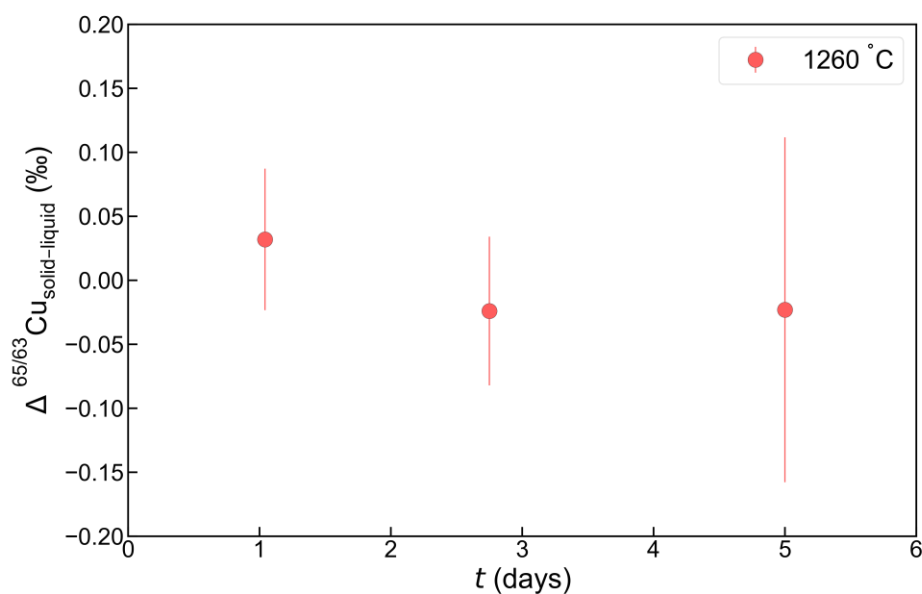


Figure S-3 Copper isotope fractionation factor for the time-series of experiments conducted at 1260 °C. All three experiments yielded consistent results within error from each other, indicating that Cu isotope fractionation reached equilibrium within 1 day at 1260 °C.

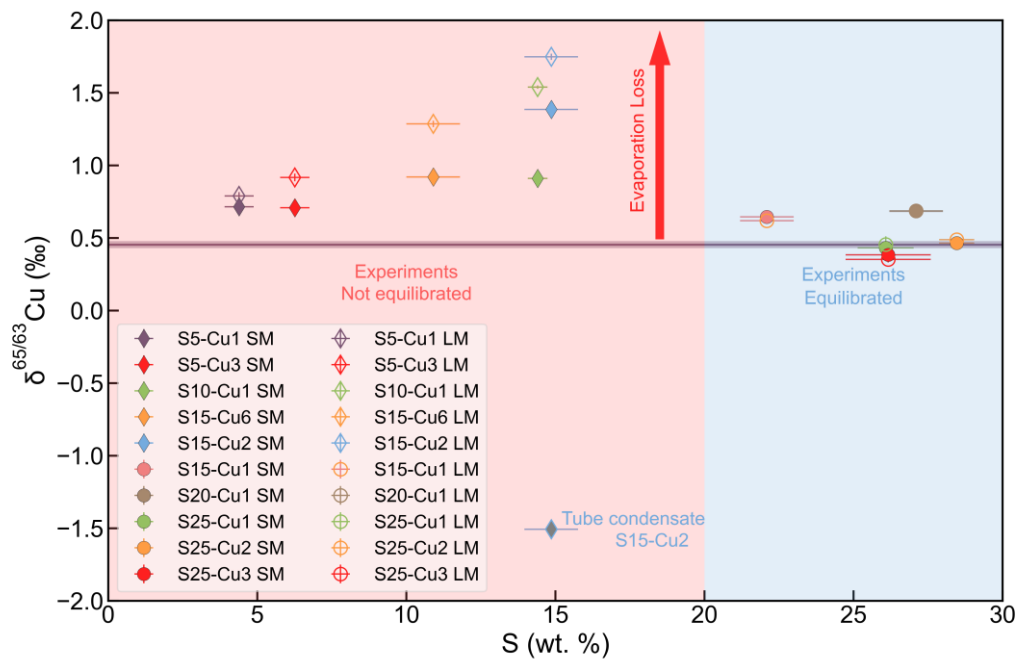


Figure S-4 Copper isotope composition of the liquid metal and solid metal for all 10 experiments conducted in this study. Initial bulk Cu composition is estimated to be 0.45 ‰ based on the Cu powder used for doping the experiments and plotted on the figure as a horizontal line.

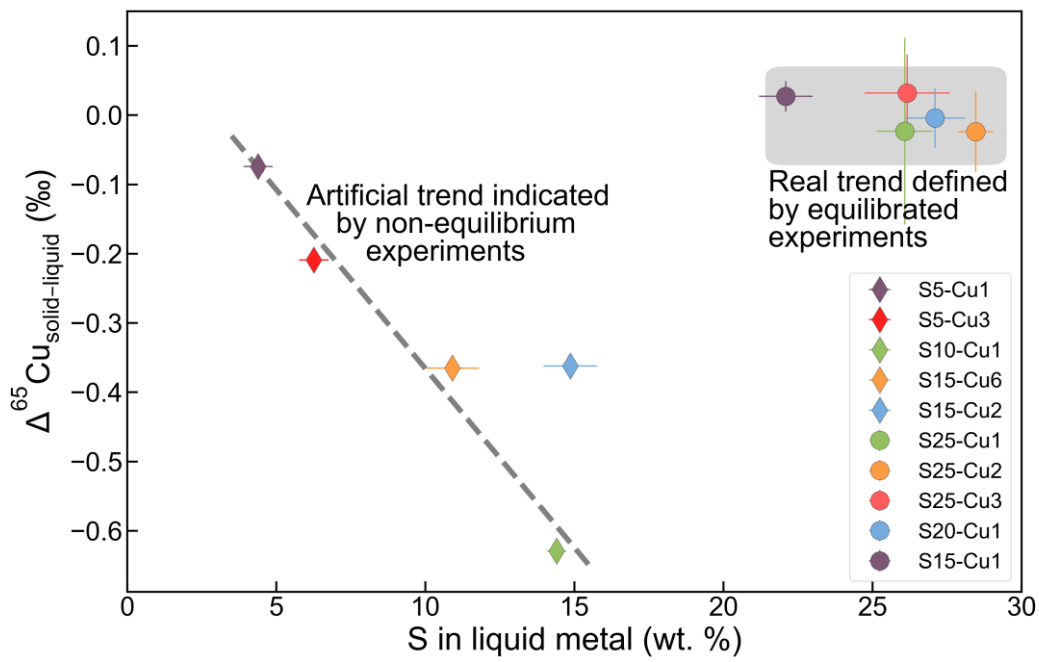


Figure S-5 Apparent Cu isotope fractionation between the solid metal and liquid metal phases directly calculated from all experiments.

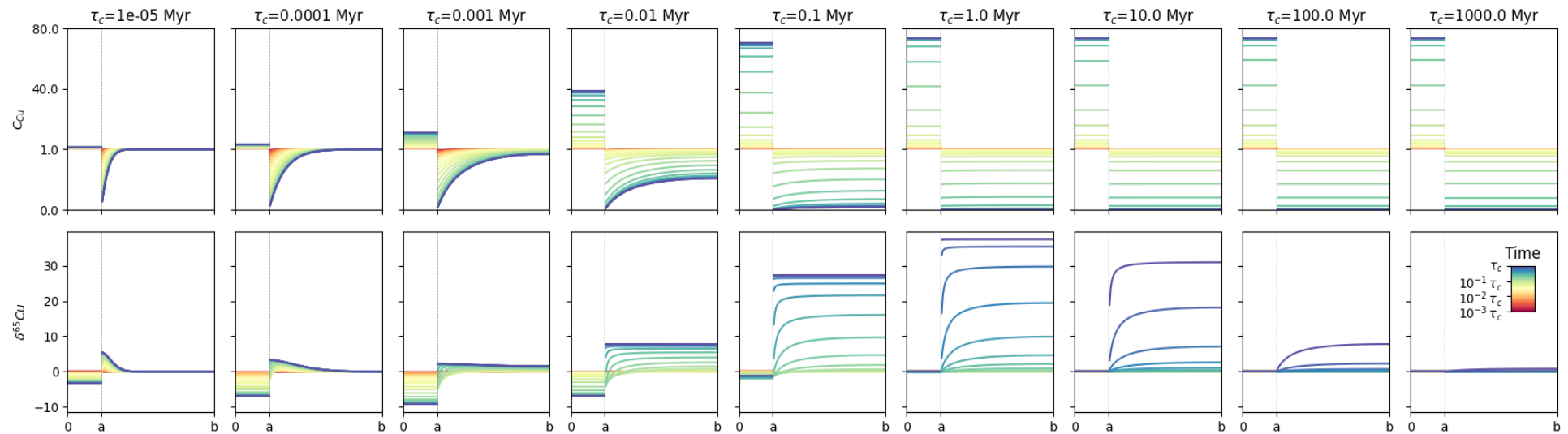


Figure S-6 Evolution of the Cu concentration and isotopic composition profiles in the troilite and metal matrix under different cooling time scales. The boundary between troilite and metal is marked using a dashed vertical curve. Copper concentration is unitless while $\delta^{65}\text{Cu}$ is in per mil. The profiles in each column show the results from models with different cooling rates from extremely high ($\tau_c = 10 \text{ yr}$) to extremely low ($\tau_c = 1 \text{ Gyr}$) values. The model assumes a troilite radius of 2 mm, metal matrix radius of 10 mm, and a temperature dependence for partition coefficient (B) of $-75,000$. The β value used for Cu diffusion is 0.5. More details about the model are available in the supplementary discussion.

Supplementary Information References

- Chabot, N.L., Jones, J.H. (2003) The parameterization of solid metal-liquid metal partitioning of siderophile elements. *Meteoritics and Planetary Science* 38, 1425–1436. <https://doi.org/10.1111/j.1945-5100.2003.tb00248.x>
- Chabot, N.L., Saslow, S.A., McDonough, W.F., Jones, J.H. (2009) An investigation of the behavior of Cu and Cr during iron meteorite crystallization. *Meteoritics and Planetary Science* 44, 505–519. <https://doi.org/10.1111/j.1945-5100.2009.tb00747.x>
- Chabot, N.L., Wollack, E.A., McDonough, W.F., Ash, R.D., Saslow, S.A. (2017) Experimental determination of partitioning in the Fe-Ni system for applications to modeling meteoritic metals. *Meteoritics and Planetary Science* 52, 1133–1145. <https://doi.org/10.1111/maps.12864>
- Cherniak, D.J. (2010) Diffusion in Carbonates, Fluorite, Sulfide Minerals, and Diamond. *Reviews in Mineralogy and Geochemistry* 72, 871–897. <https://doi.org/10.2138/rmg.2010.72.19>
- Dauphas, N., Roskosz, M., Alp, E.E., Golden, D.C., Sio, C.K., Tissot, F.L.H., Hu, M.Y., Zhao, J., Gao, L., Morris, R.V. (2012) A general moment NRIXS approach to the determination of equilibrium Fe isotopic fractionation factors: Application to goethite and jarosite. *Geochimica et Cosmochimica Acta* 94, 254–275. <https://doi.org/10.1016/j.gca.2012.06.013>
- Dauphas, N., John, S.G., Rouxel, O. (2017) Iron Isotope Systematics. *Reviews in Mineralogy and Geochemistry* 82, 415–510. <https://doi.org/10.2138/rmg.2017.82.11>
- Moeller, K., Schoenberg, R., Pedersen, R.-B., Weiss, D., Dong, S. (2012) Calibration of the New Certified Reference Materials ERM-AE633 and ERM-AE647 for Copper and IRMM-3702 for Zinc Isotope Amount Ratio Determinations. *Geostandards and Geoanalytical Research* 36, 177–199. <https://doi.org/10.1111/j.1751-908X.2011.00153.x>
- Ni, P., Macris, C.A., Darling, E.A., Shahar, A. (2021) Evaporation-induced copper isotope fractionation: Insights from laser levitation experiments. *Geochimica et Cosmochimica Acta* 298, 131–148. <https://doi.org/10.1016/j.gca.2021.02.007>
- Salje, G., Feller-Kniepmeier, M. (1977) The diffusion and solubility of copper in iron. *Journal of Applied Physics* 48, 1833–1839. <https://doi.org/10.1063/1.323934>
- Savage, P.S., Moynier, F., Chen, H., Shofner, G., Siebert, J., Badro, J., Puchtel, I.S. (2015) Copper isotope evidence for large-scale sulphide fractionation during Earth's differentiation. *Geochemical Perspectives Letters* 1, 53–64. <https://doi.org/10.7185/geochemlet.1506>
- Shahar, A., Elardo, S.M., Macris, C.A. (2017) Equilibrium Fractionation of Non-traditional Stable Isotopes: an Experimental Perspective. *Reviews in Mineralogy and Geochemistry* 82, 65–83. <https://doi.org/10.2138/rmg.2017.82.3>
- Shread, E.E., Chabot, N.L., Hamill, C.D., Ash, R.D., Corrigan, C.M. (2024) The crystallization of iron meteorites and the effect of troilite on trace element chemistry. *55th Lunar and Planetary Science Conference*, abstract #1024. <https://www.hou.usra.edu/meetings/lpsc2024/pdf/1024.pdf>
- Williams, H.M., Archer, C. (2011) Copper stable isotopes as tracers of metal-sulphide segregation and fractional crystallisation processes on iron meteorite parent bodies. *Geochimica et Cosmochimica Acta* 75, 3166–3178. <https://doi.org/10.1016/j.gca.2011.03.010>
- Xia, Y., Kiseeva, E., Wade, J., Huang, F. (2019) The effect of core segregation on the Cu and Zn isotope composition of the silicate Moon. *Geochemical Perspectives Letters* 12, 12–17. <https://doi.org/10.7185/geochemlet.1928>
- Young, E.D., Galy, A., Nagahara, H. (2002) Kinetic and equilibrium mass-dependent isotope fractionation laws in nature and their geochemical and cosmochemical significance. *Geochimica et Cosmochimica Acta* 66, 1095–1104. [https://doi.org/10.1016/S0016-7037\(01\)00832-8](https://doi.org/10.1016/S0016-7037(01)00832-8)